Pure Appl. Geophys. 181 (2024), 1181–1194

https://doi.org/10.1007/s00024-024-03441-z

Pure and Applied Geophysics

The Effects of Layer-Induced Elastic Anisotropy on Microseismic Monitoring Records in Underground Coal Mines

Liliya Malovichko[1]

Abstract—Real-time microseismic observations are extensively used in underground hard rock mines. However, microseismic monitoring in coal mines is not common. In this study, the features of microseismic (MS) event waveforms were discussed under conditions of thin-layered sedimentary media. The possibility of source mechanism evaluation was considered for the MS event recorded in coal mine. Moment tensor (MT) inversion of the waveforms can be challenging due to influence of thin-layered medium structure. Splitting of shear SH- and SV-waves is one of the characteristic features that affect MS records in coal mines. The effect of splitting was demonstrated using real microseismic data collected by an underground seismic array installed in the Polosukhinskaya coal mine, Russia. Velocities of shear SH- and SV-waves were estimated from travel times. The results reveal significant variations in shear wave velocities composed of a radial anisotropy of 75%, thus confirming the importance of a thin-layered model for moment tensor inversion. The thin-layered model was built for geological conditions at the Polosukhinskaya coal mine and synthetic seismograms were generated using QSEIS (Pyrocko OS). A full moment tensor of a single typical event was found employing the layered 1D velocity model.

Keywords: Coal seam, shear wave splitting, layer-induced elastic anisotropy, microseismic monitoring.

1. Introduction

Coal mining remains more dangerous than other kinds of mining. Underground coal mining is challenging due to coal and gas outbursts, spontaneous combustion in goaf and water inundation. Different monitoring techniques are being developed to enhance the safety and efficiency of mining operations. Real-time microseismic (MS) monitoring is one of the key monitoring methods used in underground hardrock and coal mines. MS monitoring requires an array of sensors (preferably installed in boreholes), data acquisition modules, signal processing, seismological analysis and interpretation. MS monitoring data recorded in coal mines environment are used successfully by seismologists. Some experience has been accumulated in working with these data. There are number of publications on the related topic. A few examples may clarify their contributions.

Smith et al. (1974) analysed a possible relationship between earthquakes and mining using microearthquake and acoustic monitoring data from the coal mines of Utah. By analysing the results of MT inversion, the possible connection of local seismic events with regional tectonic stress was found.

Rudajev et al. (1986) statistically analysed the data recorded in the areas of Poland and Czechoslovakia coal mines in order to understand the rockburst source mechanism. The outcome of the analysis was tested by means of physical modeling (Ŝilený et al. 1985), which resulted in combined shear-implosive mechanisms.

The source mechanism related to a large gas outburst at Sanagawa (Japan) coal mine was investigated by Sato and Fujii (1989). This event happened at a face of a crosscut straight after a coal seam was outcropped by a blasting. The shape of the analysed ejected zone located along the normal fault suggested an influence of this fault on the gas outburst. Moment tensor inversion of fourteen events was evaluated. The results of the source mechanisms interpretation suggested possible right-lateral faulting of the normal fault initiated the gas outburst.

Leake et al. (2017) used MS data recorded in a coal mine based in the Eastern United States.

[1] School of Minerals and Energy Resources Engineering, University of New South Wales, Randwick, NSW 2052, Australia. E-mail: l.malovichko@student.unsw.edu.au; liliya.r.malovichko@gmail.com

Researchers observed the seismic activity rate which correlated with the roof geology and depth of cover, but not the magnitude of the recorded events. Based on the analysis of the direction of the P-waves first motion, a focal mechanism solution was evaluated for the number of events. A uniform velocity model was assumed. The observed results indicate that stress relief resulting in dilational events occur at significant depths, 150–200 m beneath the active mining face.

Three essential characteristics of MS records in coal mine environments were discussed by King (2005): (1) The presence of reflection waves due to large impedance contrasts between host rock and coal seam. Reflection waves often overlap with direct waves. (2) Waveforms affected by the presence of near-field effects due to low-velocity mediums in mine scale observations. (3) Strong S-wave splitting due to the finely layered nature of the sedimentary medium, confirmed by the examination of borehole log data showing the presence of fine layering (tens of cm or less) of shales and sandstones in the sedimentary sequence. Due to the above-listed characteristics, attempts of moment tensor inversion were unsuccessful. The inversion provided inconsistent results and the author suggested correcting the modeling of the waveforms and removing propagation effects from seismic waveforms. S-waves splitting described by King (2005) significantly complicates the process of inversion of seismic records. The commonly used isotropic model of the medium does not provide splitting on synthetic seismograms but the ill-fitting of observed and synthetic waveforms.

Several studies devoted to multi-layered anisotropy were compared and analyzed in the work of Shen and Gao (2021). The authors discussed the advantages and limits of the present methods to study multi-layered anisotropy by local and teleseismic splitting. As it was stated by Shen and Gao, the calculation of multi-layered anisotropy is applicable only for two-layer model. However, in mining environments seismologists deal with shorter source–receiver distances and, with thinner layers of coal-bearing formation.

Apart from the difference in scale, the constantly changing environment will impact the process of MT inversion. Some of the coal seams continue to be mined out as mining progresses, others can be wedged out. Moreover, seismic activity, accompanying the excavation of coal, manifests in high amount of discrete MS events. It is essential to evaluate significant events source mechanisms in closer (few hours after the events) to real time regime. MT inversion implemented for homogeneous isotropic medium model and streamlined in hard rock mines is employing a simple analytical approach. The inversion of MT in the isotropic medium can be done using analytical Green's Function (GF) calculated 'on fly' for each microseismic event. In the case of a thin-layered medium model, the calculation of the GFs for each event will be numerically expensive. Thus, utilization of the pre-computed GFs can be a good solution. One will not need to calculate the GFs for each microseismic event. Changes in the conditions of coal mine environment (e.g., related to progress of the mining) should be considered and, the library of pre-calculated GFs should be updated (e.g., once a month) as suggested in the work of Heimann et al. (2019).

In this article, the effect of shear-wave splitting is represented in the context of layered anisotropy. One possible method of moment tensor inversion based on a fine-layered model is presented. Theoretical calculations (Rytov, 1956) of the initial parameters are used to build a thin-layered model. The pre-computed GFs store approach (Heimann et al., 2019) was used for the MT inversion. The performance of the proposed strategy is evaluated on the event of Hanks and Kanamori (1979) magnitude $M_{HK} = 1.4$ records from an underground MS array installed in the Polosukhinskaya coal mine (Russia).

2. *Applicability of Layered Anisotropy*

Three characteristics of MS records in coal mines (discussed by King (2005) as described above) are investigated for MS data recorded in the Polosukhinskaya coal mine (Russia). The projection of the MS system array on the plan view of Level 26a is shown in Fig. 1.

The first characteristic discussed by King (2005) is the near-field effect. This effect will have a notable impact on the waveforms in the case of a

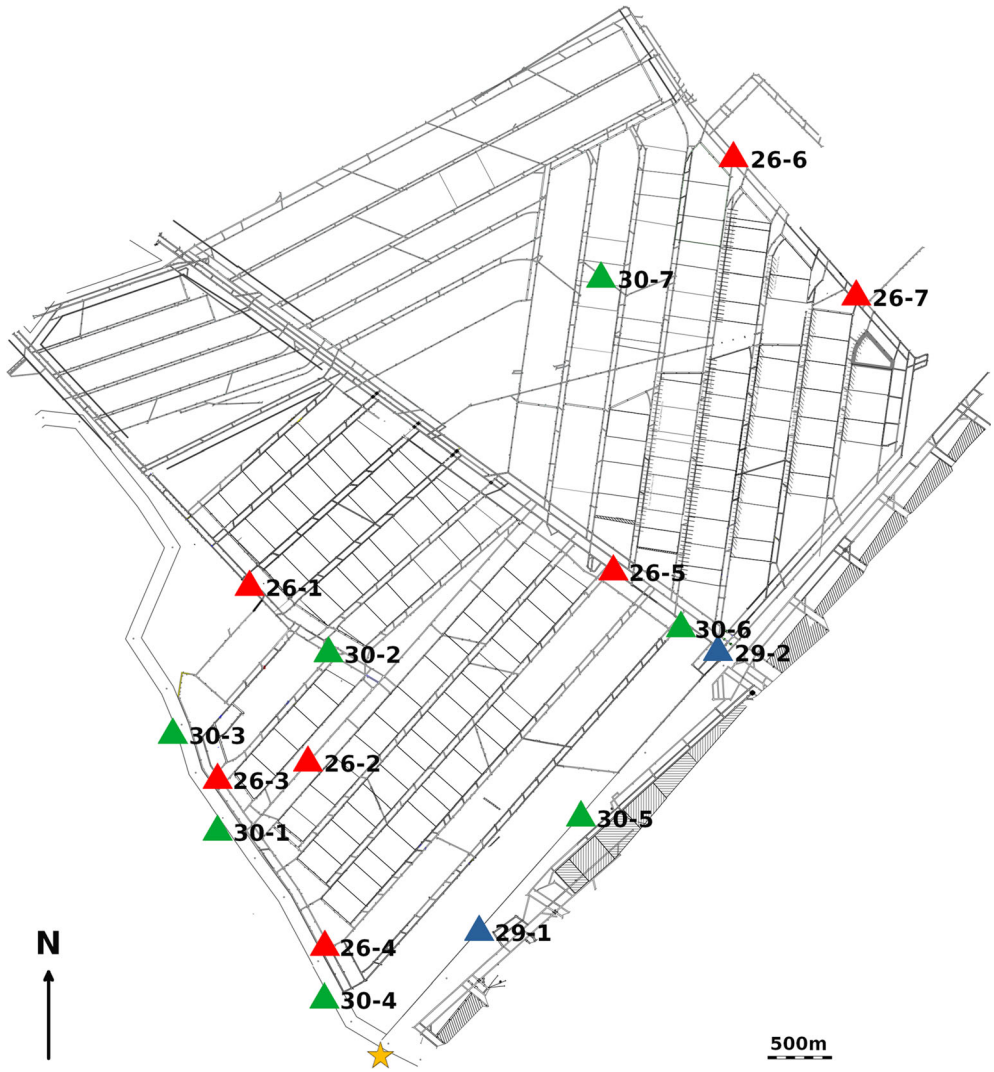

Fig. 1
The projection of the MS system array on a plan view of Level 26a at the Polosukhinskaya coal mine. The system consists of 16 tri-axial (4.5 Hz) geophones installed in three levels (26a, 29a and 30) with a maximum distance of $\sim$ 4700 m between sites. Sites installed on Level 26a are shown in red triangles. Blue and green triangles denote sites installed on levels 29a and 30, respectively. The $M_{HK}1.4$ event (indicated by a star) recorded on 2020-05-08 @ 19:01:42 by sites 30-3, 26-3, 26-2, 30-1, 29-1, 26-4, 30-4 and 30-5

locally deployed MS array only, for example, in a case of an MS array installed around a single long wall. Deploying more sparse, larger-scale MS arrays with longer source-receiver distances will help to avoid this problem. Thus, the scale of MS arrays installed at the Polosukhinskaya mine is about 3×5 km (Fig. 1), with source-receiver distances varying from 200 to 3000 m that allow us to neglect the near-field effects. Regarding the influence of reflection waves, it will be difficult to separate their effect from the complex structure of the signal, consisting of reflected, refracted and direct waves. The following results of modeling and inversion will be based on the presupposition of the presence of refraction and reflection waves in the inverted signal. Shear-wave (SH- and SV-waves) splitting is another characteristic of MS records in coal mines described by King (2005). An example of typical seismograms

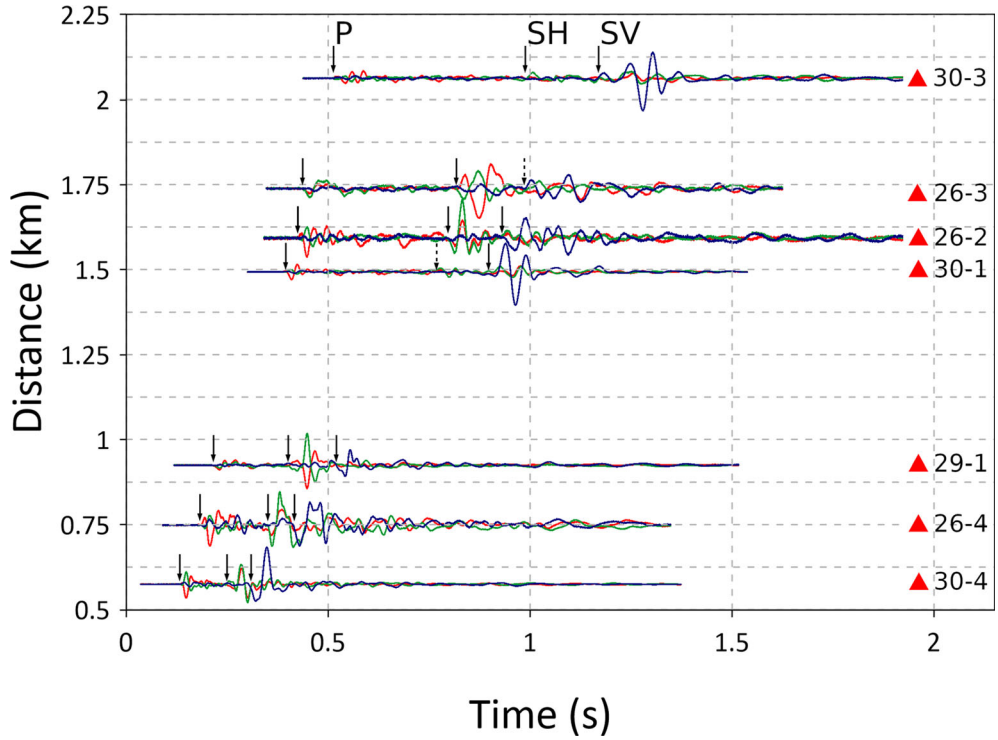

Fig. 2
An example of typical waveforms for coal mines of an $M_{HK}1.4$ event recorded on 2020-05-08 @ 19:01:42. The event was registered by eight sites. No seismograms are presented for station 30-5, as it is based too close (19 m) to station 11. Seismograms recorded on *XYZ* components (shown in red, green and blue correspondingly) with source-station distances varying from 575 to 2056 m; data is filtered between 4 and 20 Hz. All seven seismograms are showing shear-waves splitting increasing with epicentral distance

from the Polosukhinskaya coal mine is shown in Fig. 2.

As we can see, shear-wave splitting has a pronounced effect on wave data, distinct from the two above-mentioned characteristics (near-field effect and influence of reflection waves). It is worth mentioning, however, that in anisotropic media, we are dealing with quasi-P, quasi-SH and -SV waves, and not pure waves.

There are many publications describing types of anisotropy responsible for shear-wave splitting. Crampin (2020) attributes splitting to such solids as aligned crystals or aligned microcracks. He considers the splitting as a process of seismic shear-waves propagating through anisotropic solids and splitting into two phases with different velocities. According to Crampin the polarizations are strictly orthogonal for phase-velocity propagation, and approximately orthogonal for group-velocity propagation. One of the major difficulties is that observations of shear-wave splitting are path-integration phenomena that give no indication of where the anisotropy is located along the ray path, nor its extent or strength.

Another type of anisotropy potentially affecting MS data is fine-layered anisotropy. Due to the sedimentary origin, the coal and host rock, are both primarily layered. In order to substantiate this assumption, shear-wave splitting using real seismic events was estimated.

2.1. *Assessment of Shear-Wave Splitting Above Real Seismic Events*

Seismic birefringence or time-delay in shear-wave splitting appears as a result of the difference in the velocities of shear-waves. The arrival times of each split shear-wave can be read accurately. A total of 466 real events with magnitudes $m > 1.0$ recorded

between 15th February and 27th of May 2020 were used to build the travel time curves of P-SH- and SV-waves (Fig. 3). The results reveal significant variations in shear wave velocities comprising a radial anisotropy of 75%.

The following velocities of direct waves were estimated from travel times: V_P = 3666 m/s; V_{SH} = 2043 m/s and V_{SV} = 1563 m/s. When the presence of shear-wave splitting is proven, it is of interest to represent the geological media by a fine-layered model and confirm it is responsible for shear-wave splitting.

2.2. *Model Parameters Estimation*

The expression for seismic velocity of layered medium as functions of elastic properties and thickness of layers obtained by Rytov (1956) was used. According to Rytov, a medium consisting of two homogeneous and isotropic alternating materials (layer I with thickness a and Layer II with thickness b) will behave as a homogeneous anisotropic medium. This statement is true for sufficiently thin layers in relation to wavelength. The thicknesses of alternating layers can be changed arbitrarily, as long as the condition of thinness of these layers remains extant.

Accordingly, in the following equations n and $\overline{n}$ are the relative thicknesses of the stiffer and softer layers. They are related to the case of limited fine-layered medium and, a and b included only in the form of relative thicknesses of layers I and II:

$$n = \frac{a}{a+b}, \overline{n} = \frac{b}{a+b}.$$

The effective elastic moduli parameters (Lame coefficients λ and μ) of a fine-layered medium were derived by Rytov with the assumption of periodic recurring layers. Thus, the wave propagation solution was reduced to equations with periodic coefficients. A single solution for all thin layers is feasible, as the parameters inside the layers are constant and change abruptly only at the boundaries between layers. The following equations were given for an average medium density $\widetilde{\rho}$, squares of compression velocities V_P and shear-wave velocities V_{SH}, V_{SV}:

$$\widetilde{\rho} = n\rho + \overline{n}\overline{\rho},$$

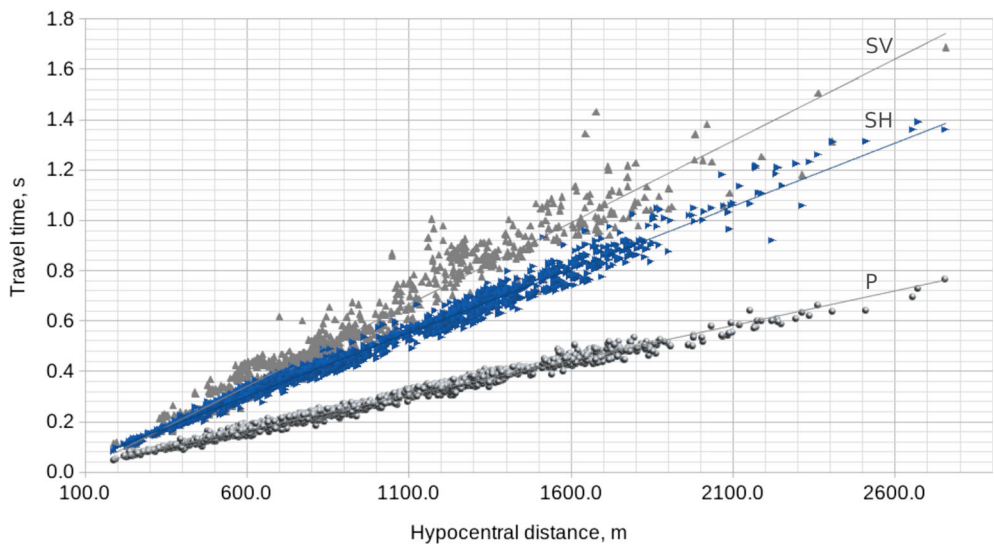

Fig. 3
Travel times of P-, SH- and SV-waves, derived from 466 real events with magnitudes $m > 1.0$ recorded between the 15th of February and 27th of May 2020

$$V_P^2 = \frac{1 + 4n\overline{n}\frac{(\mu-\overline{\mu})\left(\lambda+\mu-\overline{\lambda}-\overline{\mu}\right)}{(\lambda+2\mu)\left(\overline{\lambda}+2\overline{\mu}\right)}}{\overline{\rho}\left(\frac{n}{\lambda+2\mu}+\frac{\overline{n}}{\overline{\lambda}+2\overline{\mu}}\right)},$$

$$V_{SV}^2 = \frac{1}{\widetilde{\rho}\left(\frac{n}{\mu}+\frac{\overline{n}}{\overline{\mu}}\right)},$$

$$V_{SH}^2 = \frac{n\mu + \overline{n\mu}}{\widetilde{\rho}}.$$

These equations were used in order to select such values of the interval velocities in layers I and II, which give the nearest to real values of direct wave velocities (V_P = 3666 m/s, V_{SH} = 2043 m/s and V_{SV} = 1563 m/s), derived from travel times in Fig. 3. Thus, the following interval velocities and density values were obtained: V_P^I = 3840 m/s, V_S^I = 2330 m/s, ρ^I = 2.6 g/cm^2 and V_P^{II} = 2470 m/s, V_S^{II} = 1450 m/s, ρ^{II} = 1.3 g/cm^2. Lithological Index I represent the average properties of the adjacent strata (siltstone, sandstone and the remaining sediments) and II—the coal seam.

These derived values were employed as input to generate elementary seismograms using Wang's (1999) code QSEIS. QSEIS features functionality to calculate GFs for a homogeneous or a layered elastic half-space. Each layer of the layered elastic half-space is assumed to be homogeneous and isotropic. Method uses an orthonormal propagator algorithm to calculate the seismogram for layered viscoelastic half-space model. It is known as a numerically stable method. An example of the seismograms calculated by this method is shown in Fig. 4. Synthetic seismograms were generated from a double-couple source with the following parameters: magnitude of 6.0, a strike of − 45°, a dip of 70° and a rake of − 90°. They have clear arrivals of P-, SH- and SV-waves. Direct wave velocities, derived from travel times, have the following values: V_P = 3636 m/s, V_{SH} = 2051 m/s and V_{SV} = 1544 m/s.

Thus, the travel time velocities obtained from the real events database (Fig. 3) are quite close to those assessed from synthetic seismograms calculated for a layered half-space (Fig. 4, first seismogram from the top). A deviation between travel time velocities values is no more than 1.2%, which is proving that the Rytov's method is acceptable, and the model can be customised and used further for MT inversion.

It is common in hardrock mine seismology to conduct MT inversion by using isotropic homogeneous model. In crustal seismology a thick (compared to wavelength) layered model is often used to generate Green's functions. However, there are cases when the wavelength is much greater than the layer thickness, and both isotropic homogeneous and thick layered model will not work for MT inversion, particularly in the case of coal mine MS records.

3. Customisation of the Effective Model

3.1. Geology

In this chapter, the data collected from the Polosukhinskaya coal mine will be considered. The mine is located within the Baidaevskae deposit (Kuzbass, Russia), represented by a large brachysyncline structure made of coal-bearing strata with a thickness reaching ∼ 1300 m. Within the mine field the coal-bearing measures occur in the sediments with a thickness of 900 m. They are characterized by frequently interbedding sandstones and argillaceous varieties—siltstones and mudstones. These geological formations contain numerous (> 300) thin coal seams, ranging in thickness from centimeters to 5 m. Only 45 of them are productive in terms of coal quality and thickness of seam (> 1.5 m). These 45 coal seams have serial numbers that increase from bottom to top and thicknesses within the range of 1.5–2 m, with only a few of them reaching 3–5 m. Thus, for example, coal seam 29a has a thickness of 3.5 m. The thinner coal seams are interbedded with the host rocks and grouped into packs. It is possible that they exhibit the overall anisotropy effect. The task of reproducing a detailed model was not set and, it might be unreachable due to the lack of detailed geological information.

3.2. Data

It is of interest to describe the geometry of the mine and MS array. The ∼ 900 m coal suite is represented by a fine stratigraphic layering of

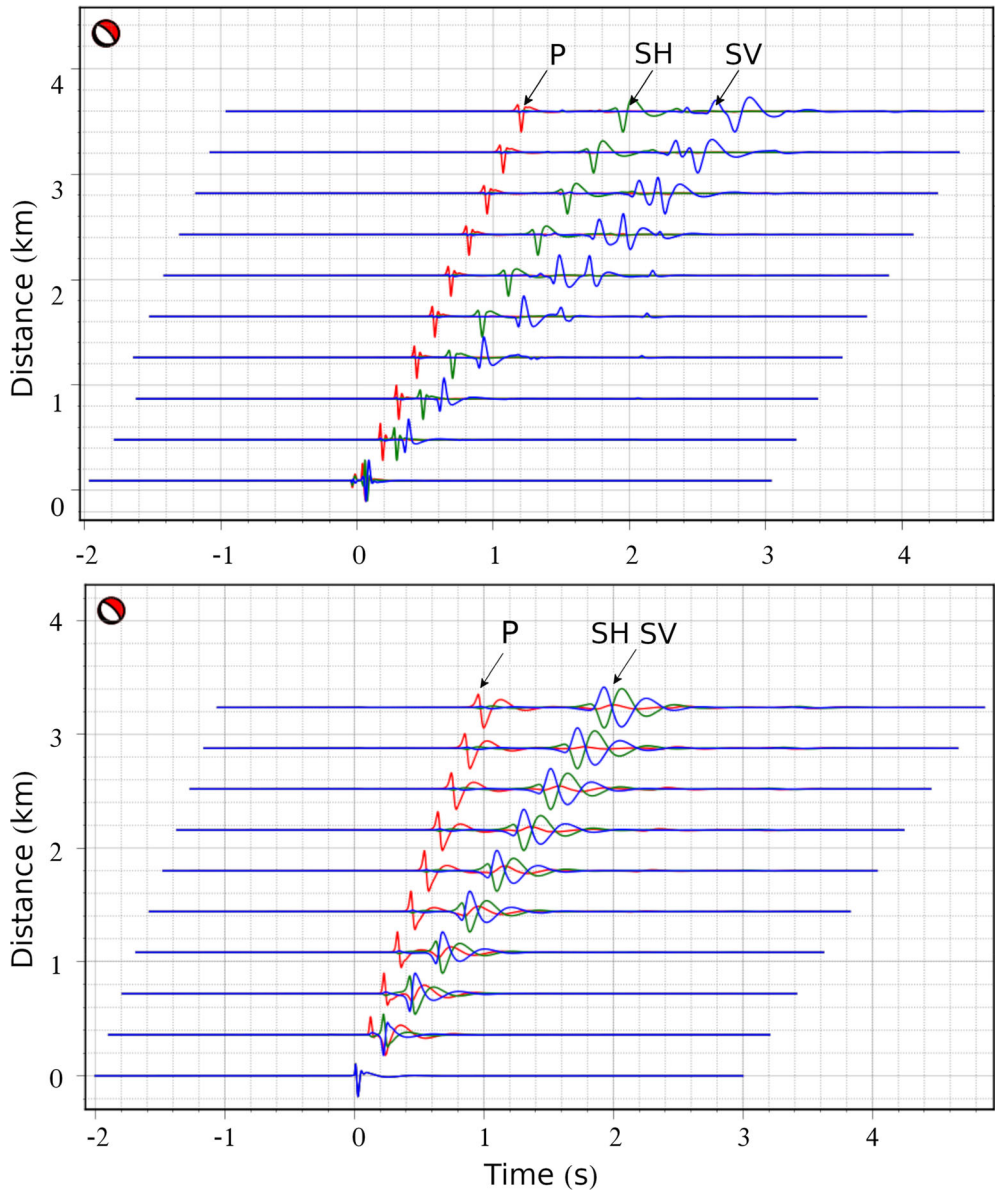

Fig. 4
Synthetic seismograms of displacement in a frequency range of 2.5–27.5 Hz from a double couple MS source with an impulse length of 0.25 s. The source has a strike of − 45°, a dip of 70° and a rake of − 90°. The vertical components are shown in blue (Down) and the horizontal components (East) are shown in green and red (North). The maximum source-receiver distance is 4 km. The above seismogram demonstrates the anisotropy effect (splitting of S-waves), while the seismogram below demonstrates the effect of a simple isotropic model. The anisotropy effect is achieved by interbedding of homogeneous isotropic thin (3 m) layers. The layers describe the properties with Lithological Indexes I and II and are derived using Rytov's equations

medium-grained sandstone (21.3%), fine-grained siltstone and mudstone (61.1%), coal seams (4.2%) and remaining sediments (13.4%). Three coal seams are currently being mined and corresponding to levels 30, 29a and 26a. Longwall mining development and tunneling are carried out at the mine alternately in these three levels. Level 30 has an average thickness of 2.14 m. Level 29a lies 60–70 m below level 30

Table 1

Velocity model with a 10 m soft-soil layer on the surface

Index	Layer thickness, m	Depth interval, km	V_P, km/s	V_S, km/s	ρ, g/cm^3	Q_P	Q_S
Weathered zone	10	0.000–0.010	2.37	1.35	1.2	1	0.5
I	3	0.010–0.013	3.84	2.33	2.4	20	10
II	3	0.013–0.016	2.47	1.45	1.3	20	10
…	…	…	…	…	…	…	…
II	**3**	**0.418–0.421**	**2.47**	**1.45**	**1.3**	**20**	**10**
I	**3**	**0.421–0.424**	**3.84**	**2.33**	**2.4**	**20**	**10**
II	**3**	**0.424–0.427**	**2.47**	**1.45**	**1.3**	**20**	**10**
I	**33**	**0.427–0.460**	**3.84**	**2.33**	**2.4**	**20**	**10**
II	**4**	**0.460–0.464**	**2.47**	**1.45**	**1.3**	**20**	**10**
I	**47**	**0.464–0.511**	**3.84**	**2.33**	**2.4**	**20**	**10**
II	**3**	**0.511–0.514**	**2.47**	**1.45**	**1.3**	**20**	**10**
…	…	…	…	…	…	…	…
II	3	0.898–0.901	2.47	1.45	1.3	20	10
I	3	0.901–0.904	3.84	2.33	2.4	20	10
Lower half-space	∞	0.904–∞	4.3	2.5	2.6	20	10

Index I represent the average properties of the adjacent strata (siltstone, sandstone and remaining sediments) while Index II represents coal seam properties (highlighted in gray). Depth interval of 418–514 m is representing the mine field. It is described in more detail due to availability of geological information, in particular on the thickness of the coal seams. The geometry and properties of this part of the model is represented in the middle of the table in a bold font

and has an average thickness of 2.9 m. Level 26a lies 120–140 m below level 29a and has an average thickness of 2.0 m. All levels of the mine are considered hazardous by rock bursts from a depth of 190 m, and by coal and gas outbursts from a depth of 300 m. This motivated the installation of MS monitoring systems in this mine.

The underground MS array was installed mine-wide with a maximum distance of $\sim$ 4.7 km between sites. Hypocentral distances of the registered microseismic events vary between 0.2 and 3 km. A relatively thin coal suite and fine stratigraphic layering versus wavelength (below the tuning thickness $<\lambda/4$) allows to conceptually designate the medium as vertical transverse isotropic (VTI). Another feature to be mentioned is the scale of the mine and the corresponding MS array—wide in the lateral direction, and thin in the vertical direction—which imposes uncertainties on the vertical location of events.

3.3. Model

Due to the peculiarities of the stratigraphic layering described above and the lack of detailed geological information, it is evident that the task of reproducing an explicit model is not a viable option. Thus, considering the coal seam geometry and the results of the field study described by Kurbatova (1959), a one-dimensional (1D) density (ρ), compressional and shear wave velocity (V_P, V_S) model was built using petrophysical properties that were estimated above, in Sect. 2.2.

The process of choosing the number of layers in the Model was iterative, with a series of prototypes being built to test various options. The Model represented in Table 1 was selected. In total, 274 interlayers of I and II were used for the model presented in Table 1. Most of the layers of the same thickness–3 m. First ten-meter layer represents soft-soil zone. Further, the Model describes the interbedding of thin coal and host rock layers of the same thickness, which defines the upper overburden rock. The Model within the depths of the minefield (418–514 m) is described in more detail due to availability the of geological information, in particular on the thickness of the coal seams. The geometry and properties of this part of the model is represented in the middle of the Table 1 in a bold font. The layers of host rock with thicknesses of 33 and 47 m are most likely containing much thinner interlayers of coal. As

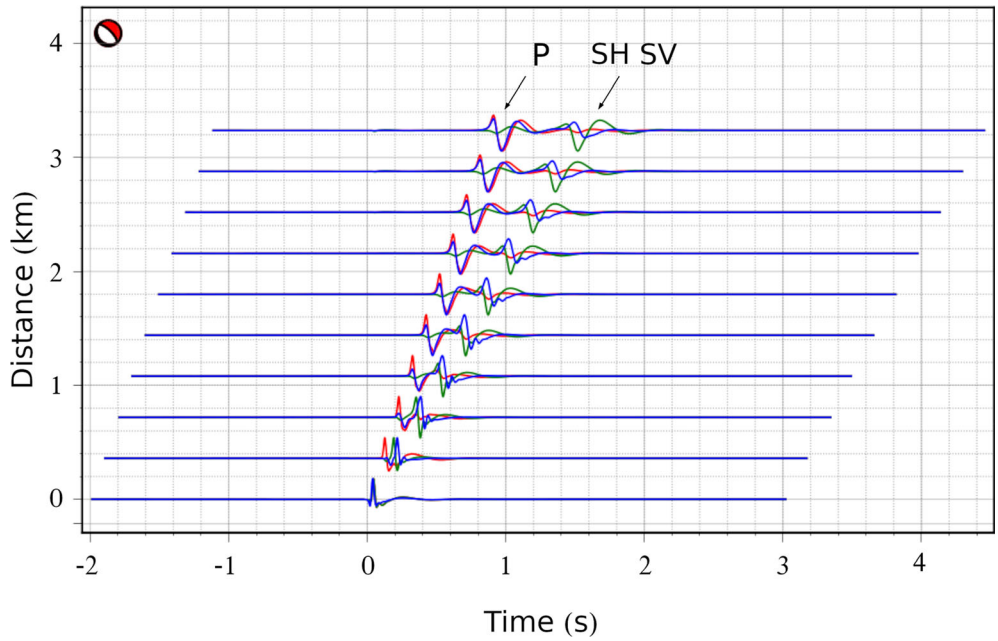

Fig. 5
Synthetic seismograms of displacement in a frequency range of 2.5–27.5 Hz, from a double couple MS source with an impulse length of 0.25 s. The source has a strike of − 45°, a dip of 70° and a rake of − 90°. The vertical (Down) components are shown in blue, and the horizontal (East and North) components are shown in green and red correspondingly. The maximum source-receiver distance is 4 km. The seismograms demonstrate the effect of anisotropic Model (Table 1)

more information becomes available the Model can be updated.

An attempt to use a model that describes coal-bearing formations around the minefield only (Table 1, 418–514 m) did not provide the desired splitting of shear waves (Fig. 5). Whilst the inclusion of thin-layered overburden and underburden strata facilitated the effect of anisotropy.

The desired splitting (Fig. 6) was achieved through iterative process of choosing the number of layers, with a series of prototypes being built to test various options.

3.4. Q-Values

An amplitude decay rate or the attenuation factor Q was determined by manual analysis of the seismograms. The waveforms calculated for different V_{SV} and V_{SH} values were analysed. Figure 7 shows the waveforms calculated for the same model but with different Q values. The smaller combination of Q values of Q_P = 20, Q_S = 10 was chosen for the Moment Tensor estimation.

4. Moment Tensor Estimation

Here, the seismic records of the event recorded on 2020-05-08 (19:01:42 UTC) and located in the Polosukhinskaya coal mine will be analysed in detail. The event features a moment magnitude of M_{HK} 1.4. It was recorded by 11 stations with epicentral distances varying from 575 to 2056 m. Each station consists of a single 4.5 Hz tri-axial geophone installed in a vertically drilled upward 10 m borehole. Figure 8 displays the event location together with the triggered stations of the IMS (Institute of Mine Seismology) network and geological structures.

Figure 2 offers an overview of the real data seismograms filtered with a Butterworth band-pass filter between 4 and 20 Hz. Red, green and blue colored seismograms represent X, Y and Z components, respectively. No seismograms are presented for

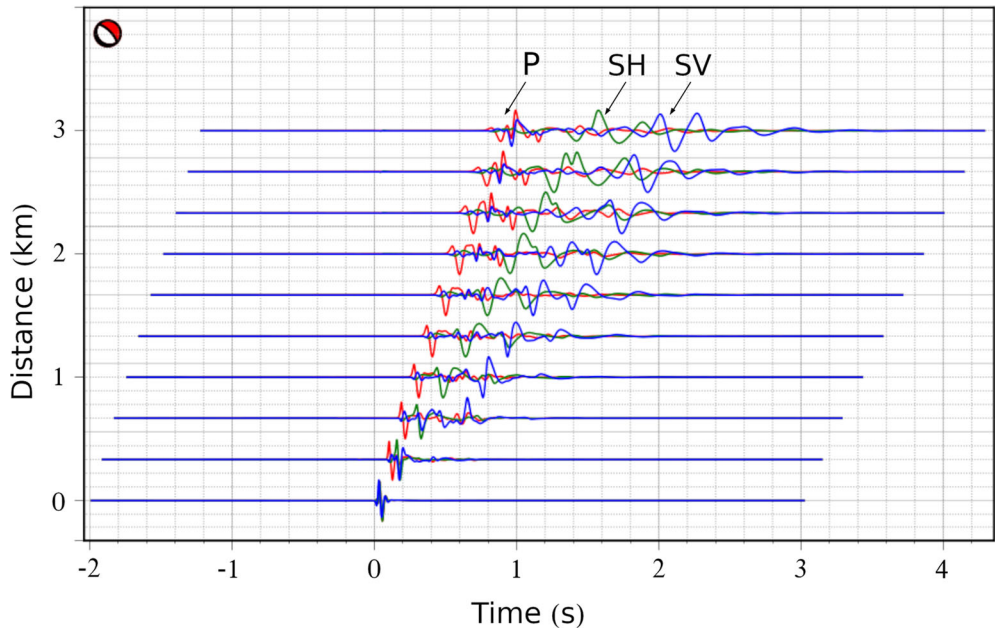

Fig. 6
Synthetic seismograms of displacement in a frequency range of 2.5–27.5 Hz, from a double couple MS source with an impulse length of 0.25 s. The source has a strike of − 45°, a dip of 70° and a rake of − 90°. The vertical (Down) components are shown in blue while the horizontal (East and North) components are shown in green and red correspondingly. The maximum source-receiver distance is 4 km. The seismograms demonstrate the effect of the anisotropic Model (Table 1)

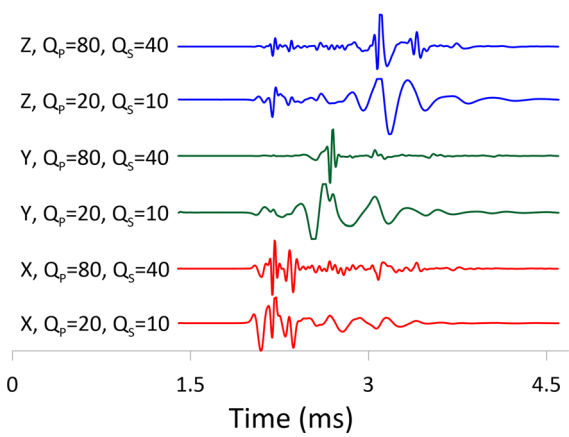

Fig. 7
Waveforms of displacement in a frequency range of 2.5–27.5 Hz, calculated for a double couple source at a 2 km distance. The DC source has a strike of − 45°, a dip of 70° and a rake of − 90°. The vertical (Down) components are shown in blue, and the horizontal (East and North) components are shown in green and red correspondingly. The seismograms demonstrate the effect of anisotropic Model for different Q values. Lower seismograms were calculated for Q_P = 20, Q_S = 10 and upper seismograms for Q_P = 80, Q_S= 40

station 5 as it is based too close (at distance of 19 m) to station 11. All seismograms of the event show shear (S-wave) wave splitting, which increases with epicentral distance. In some cases, it is impossible to separate SH- and SV-waves. These waveforms are typical of microseismic data recorded in underground coal mines. Thus, the generalised approach of analysing the event can have broad applicability in the underground coal mine environment.

In-depth analysis of microseismic events implies determining of moment tensor. Moment tensor (MT) estimation was done by calculating full-waveform synthetic seismograms for solutions provided by Wang (1999) and represented in QSEIS codes. QSEIS codes were utilised to compute the Green Function stores using Pyrocko, which is an open-source seismology toolbox and library (Heimann et al., 2019). Green Functions were computed employing a tapered wavelet, a sample rate of 500 Hz, and a grid spacing of 5 m. The databases comprise a source depth fixed at 452 m.

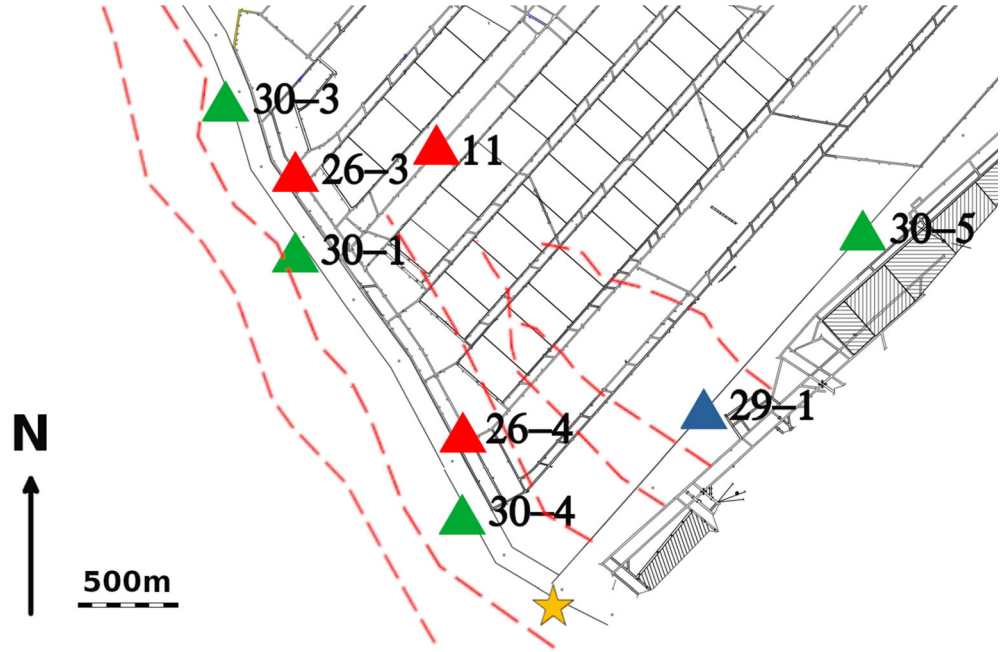

Fig. 8
The projection of geological structures (red dashed lines) and M_{HK}1.4 event (indicated by a star) recorded on 2020-05-08 @ 19:01:42 on a plan view of Level 26a at the Polosukhinskaya coal mine. Triangles represent triggered sites. Only sites that recorded the event are represented. 3D model of geological structures is not available

Due to the wide lateral spread of the seismic station array compared to the vertical, the vertical variations of the stations were not considered. Thus, an assumption that the whole array is located on the Level 450 m was made. For each solution, only a single pulse (normalised square half-sinusoid for simulating a physical delta impulse) was used.

The best fit to the velocity waveforms was achieved using f_0 = 4 Hz, corresponding to a pulse duration of 0.25 s. Results from the inversion in the selected frequency range of 4–20 Hz in Fig. 9 provide a good fitting of synthetic (colored seismograms) and observed (gray shaded seismograms) waveforms.

The MT determined by the grid search method involves mostly a deviatoric (74%) component which corresponds to a normal faulting type mechanism. The mechanism correlates with the nearby structures (Fig. 8) in respect of the strike. It should be noted that the coverage of the event by seismic stations is insufficient. The seismic stations are concentrated in the Northeast and Northwest quadrants in relation to the source.

The combination of 4% compensated linear vector dipole (CLVD) and 22% of the isotropic (implosive) component can be explained by the influence of excavations on the source origin. Another explanation can be related to the influence of anisotropic media. According to Vavrycuk (2005) shear faulting in anisotropic rocks illustrates properties of non-DC mechanisms in dependence on strength and symmetry of anisotropy and on the orientation of faulting. The amount of the CLVD and ISO depends on strength and symmetry of anisotropy and, on the orientation of the faulting. For example, in Table 3 in Vavrycuk (2005) lists the following combination of non-DC components produced by shear faulting for periodic thin-layered model: DC 72.0%; CLVD 18.7% and, ISO 14.4%. This approximately coincides with the combination of the obtained MT components. Thus, the 26% of non-DC component can be attributed to the influence of anisotropic media.

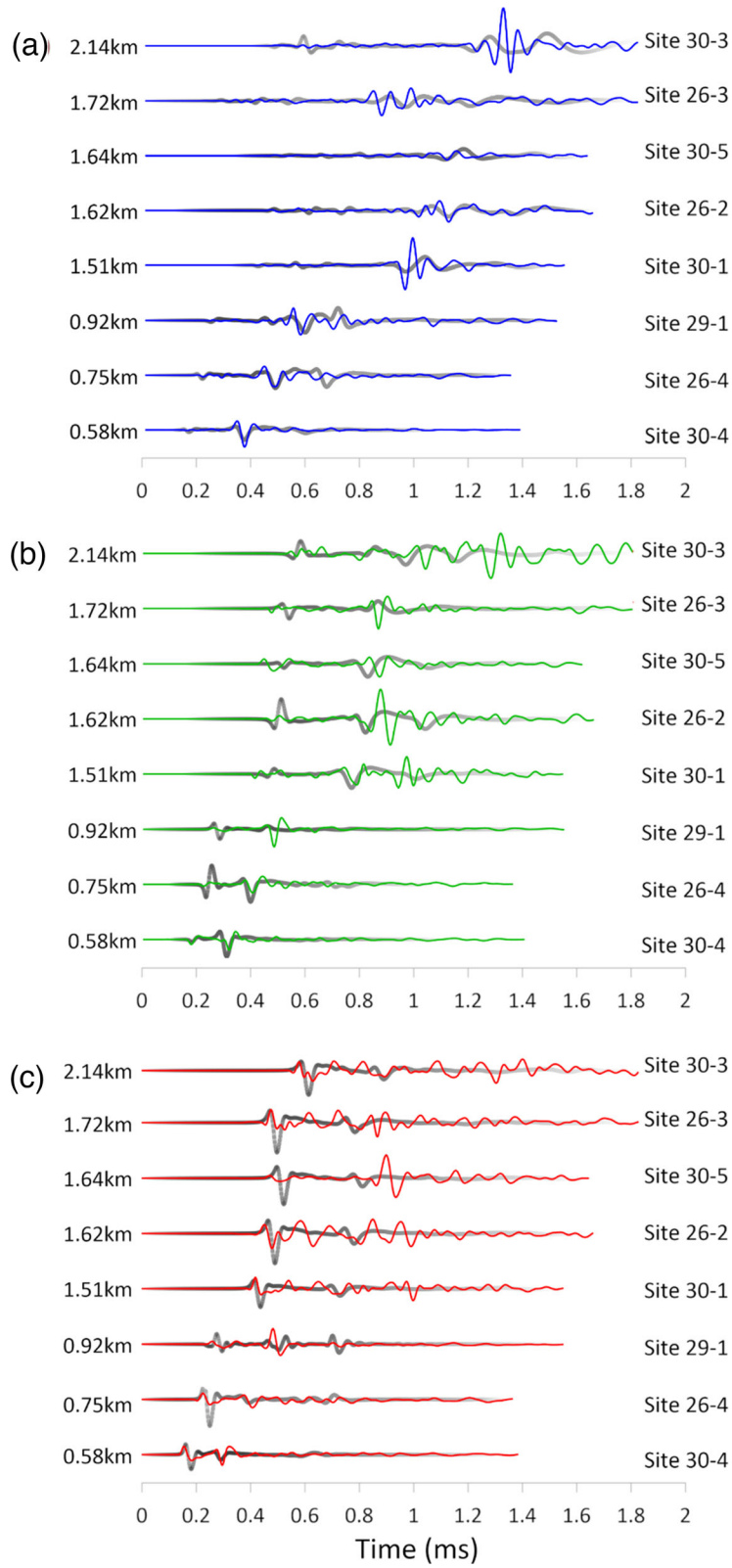
(a)
2.14km
Site 30-3
1.72km
Site 26-3
1.64km
Site 30-5
1.62km
Site 26-2
1.51km
Site 30-1
0.92km
Site 29-1
0.75km
Site 26-4
0.58km
Site 30-4
0 0.2 0.4 0.6 0.8 1 1.2 1.4 1.6 1.8 2
(b)
2.14km
Site 30-3
1.72km
Site 26-3
1.64km
Site 30-5
1.62km
Site 26-2
1.51km
Site 30-1
0.92km
Site 29-1
0.75km
Site 26-4
0.58km
Site 30-4
0 0.2 0.4 0.6 0.8 1 1.2 1.4 1.6 1.8 2
(c)
2.14km
Site 30-3
1.72km
Site 26-3
1.64km
Site 30-5
1.62km
Site 26-2
1.51km
Site 30-1
0.92km
Site 29-1
0.75km
Site 26-4
0.58km
Site 30-4
0 0.2 0.4 0.6 0.8 1 1.2 1.4 1.6 1.8 2
Time (ms)

◀ Fig. 9
Time-domain waveform fits for full moment tensor (MT) estimation compared at sensors 30-4, 26-4, 29-1, 30-1, 26-2, 30-5, 26-3 and 30-3. The real seismograms displayed in colours while the synthetic shown in grey. For each sensor, transverse and vertical components are shown (denoted by *X* in red, *Y* in green and *Z* in blue, respectively). Distances and azimuths with respect to the source are given. The colour version of this figure is available only in the electronic edition

5. Discussion and Conclusions

Splitting of shear waves is a typical characteristic feature that complicates MS waveforms and the inversion process in coal mines. Isotropic homogeneous velocity models widely used for the inversion in mine seismology cannot be employed for inversion. Instead, a thin-layered medium model can be used to describe the splitting of shear waves.

The proposed thin-layering model is reasonably optimal for meeting the goals of both describing S-waves splitting and strata conditions. Such model does not satisfy all geological conditions, as the number of coal seams may vary within the minefield. The coal seams can be mined out, pinched out, or reappear. However, the employment of a single approximate model is justified as coal mines under development are often seismically active: more than thirty large ($M_{HK} > 0.0$) MS events can be recorded daily. It is computationally demanding to calculate synthetic GF for all events (registered by different combination of receivers and various source locations) separately. Recalculation of GFs in each iteration during optimisation is also time-consuming. Therefore, efficient pre-computed storage of synthetic GFs for an optimal model enables to refine the process of MT inversion.

MT inversion was successfully applied to microseismic records of $M_{HK} = 1.4$ event. The inversion for source location was not performed. It is popular in crustal seismology to invert for more than one parameter, including determining the source location in conjunction with the mechanism. However, determining the location of the event in coal mines, especially the vertical location is a challenging task. It is challenging due to (1) source pulse-frequency content; (2) features of the geometry of the coal seam and, consequently, the geometry of the mine field and the arrangement of MS array. Both in mine seismology and in crustal seismology, the frequency composition of the source is approximately the same low frequency ($\sim$ 25 Hz). Although, the accuracy and distances traveled by waves are different: in crustal seismology, these are tens and hundreds of kilometers, and in coal mines—hundreds of meters. At the same time, due to specific distribution of MS arrays in coal mines—that is, wide in the lateral direction ($\sim$ 6000 m) compared to vertical ($\sim$ 500 m)—the vertical location of the MS event is often unreliable. In this case, source mechanism evaluation and analysis can clarify the nature of the source and thereby associate it with a certain depth of origin or lateral location, for example–vicinity to geological structures.

Acknowledgements

I wish to thank anonymous reviewers for their comments that helped to improve the quality of this article. I gratefully acknowledge Dr. Sebastian Heimann and Dr. Hannes Vasyura-Bathke for their advice on both Pyrocko and BEAT software questions. I appreciate the support from JSC "Polosukhinskaya" by facilitating access to the microseismic data catalog and permission to publish.

Funding

Open Access funding enabled and organized by CAUL and its Member Institutions. There was no funding provided or used in this research.

Data availability

The data is not available, but can be provided upon the request from the mine.

Declarations

Conflict of interest There is no competing interests.

References

Cai, W., Dou, L., Si, G., Cao, A., Gong, S., Wang, G., & Yuan, S. (2019). A new seismic-based strain energy methodology for coal burst forecasting in underground coal mines. *International Journal of Rock Mechanics and Mining Sciences, 123*(104086), 1365–1609. https://doi.org/10.1016/j.ijrmms.2019.104086

Crampin, S. (1984). An introduction to wave propagation in anisotropic media. *Geophysical Journal of the Royal Astronomical Society, 76*, 17–28.

Crampin, S. (2020). Shear-wave splitting: New geophysics and earthquake stress-forecasting. *Encyclopedia of solid earth geophysics. Encyclopedia of earth sciences series.* Springer.

Hanks, T. C., & Kanamori, H. (1979). A moment magnitude scale. *Journal of Geophysical Research, 84*(B5), 2348–2350. https://doi.org/10.1029/JB084iB05p02348

Heimann, S., Vasyura-Bathke, H., Sudhaus, H., Isken, M., Kriegerowski, M., Steinberg, A., & Dahm, T. (2019). A Python framework for efficient use of pre-computed Green's functions in seismological and other physical forward and inverse source problems. *Solid Earth Discussions, 10*, 1921–1935. https://doi.org/10.5194/se-2019-85

King, A. (2005). Source-parameter estimation in a coal environment. In *RaSiM6: Proceedings of the sixth international symposium on rockburst and seismicity in mines proceedings* (pp. 131–134). Australian Centre for Geomechanics. https://doi.org/10.36487/ACG_repo/574_8.

Kurbatova, A. (1959). To the characterization of coal seams from the upper part of the geological section of the Baidaevskoe deposit in Kuzbass. *Geology of Kuzbass, 99*, 221–227.

Leake, M. R., Conrad, W. J., Westman, E. C., Afrouz, S. G., & Molka, R. J. (2017). Mictoseismic monitoring and analysis of induced seismicity source mechanism in a retreating room and pillar coal mine in Eastern United States. *Speech Communication*. https://doi.org/10.1016/j.undsp.2017.05.002

Mendecki, A. (1999). *Seismic monitoring in mines*. Chapman and Hall.

Rudajev, V., Teisseyre, R., Kozák, J., & Ŝilený, J. (1986). Possible mechanism of rockbursts in coal mines. *Pageoph, 124*(4/5), 841–855.

Rytov, S. M. (1956). Акустические свойства мелкослоистой среды [Acoustic properties of fine-layered medium]. *Acoustic Journal, 2*(1), 71–83.

Sato, K., & Fujii, Y. (1989). Source mechanism of a large scale gas outburst at Sanagawa coal mine in Japan. *Pageoph, 129*(3/4), 325–343.

Shen, S., & Gao, Y. (2021). Research progress on layered seismic anisotropy—A review. *Earthquake Research Advances., 1*(1), 6. https://doi.org/10.1016/j.eqrea.2021.100005

Ŝilený, J., Rudajev, V., Lokajíček, T., & Kozák, J. (1985). Implosive rock bursts and their laboratory simulation. *Acta Montana, 71*, 33–48.

Smith, R. B., Winkler, P. L., Anderson, J. G., & Scholz, C. H. (1974). Source mechanisms of microearthquakes associated with underground mines in Utah. *Bulletin of the Seismological Society of America, 64*(4), 1295–1317.

Vasyura-Bathke, H., Dettmer, J., Steinberg, A., Heimann, S., Isken, M., Zielke, O., Mai, P., Sudhaus, H., & Jónsson, S. (2019). BEAT—Bayesian earthquake analysis tool. GFZ data services, V. 1.0. Retrieved from https://doi.org/10.5880/fidgeo.2019.024.

Vavrycuk, V. (2005). Focal mechanisms in anisotropic media. *Geophysical Journal International., 161*, 334–346.

Wang, R. (1999). A simple orthonormalization method for stable and efficient computation of Green's Functions. *Bulletin of the Seismological Society of America, 89*(3), 733–741.

(Received December 7, 2021, revised January 15, 2024, accepted January 29, 2024, Published online March 19, 2024)